Radiation Damage In Scintillating Crystals

Article *in* Nuclear Instruments and Methods in Physics Research Section A Accelerators Spectrometers Detectors and Associated Equipment · August 1998

DOI: 10.1016/S0168-9002(98)00498-7 · Source: OAI

1 author:

Ren-Yuan Zhu
California Institute of Technology
3,354 PUBLICATIONS **159,672** CITATIONS

ELSEVIER Nuclear Instruments and Methods in Physics Research A 413 (1998) 297–311

NUCLEAR INSTRUMENTS & METHODS IN PHYSICS RESEARCH Section A

Radiation damage in scintillating crystals

Ren-yuan Zhu*

California Institute of Technology, 1201E, California Blvd., Pasadena, CA 91125, USA

Received 2 February 1998

Abstract

Crystal Calorimetry in future high-energy physics experiments faces a new challenge to maintain its precision in a hostile radiation environment. This paper discusses the effects of radiation damage in scintillating crystals, and concludes that the predominant radiation damage effect in crystal scintillators is the radiation-induced absorption, or color center formation, not the loss of scintillation light yield. The importance of maintaining crystal's light response uniformity and the feasibility to build a precision crystal calorimeter under radiation are elaborated. The mechanism of radiation damage in scintillating crystals is also discussed. While the damage in alkali halides is found to be caused by the oxygen/hydroxyl contamination, it is the structure defects, such as oxygen vacancies, cause damage in oxides. Material analysis methods used to reach these conclusions are presented in details.

1. Introduction

Total absorption shower counters made of inorganic scintillating crystals have been known for decades for their superb energy resolution and detection efficiency. In high energy and nuclear physics, large arrays of scintillating crystals have been assembled for precision measurements of photons and electrons. The discovery potential of crystal calorimetry was earlier demonstrated by the Crystal Ball detector [1] through its study of radiative transitions and decays of the Charmonium family [2]. Over the last decade, following the Crystal Ball and CUSB [3,4] experiments, larger crystal calorimeters have been constructed, and their use has been a key factor in the successful physics programs of the L3 at LEP [5], of the CLEO II at CESR [6], and of the Crystal Barrel at LEAR [7].

Recently, several crystal calorimeters have been designed and are under development for the next generation of high-energy physics experiment. These include a CsI calorimeter for the KTeV experiment at Fermi Lab [8], two CsI(Tl) calorimeters for B Factory experiments: the BaBar experiment at SLAC [9] and the BELLE experiment at KEK [10], and a lead tungstate ($PbWO_4$) calorimeter for the Compact Muon Solenoid (CMS) experiment at the Large Hadronic Collider (LHC) [11], where the electroweak symmetry breaking physics requires resolution of the crystal calorimetry [12–14]. Table 1 summarizes design parameters for these crystal calorimeters. One

* Corresponding author. Tel.: +1 626 395 6661; fax: +1 626 795 3951; e-mail: zhu@cithex.caltech.edu.

0168-9002/98/$19.00
PII: S0168-9002(98)00498-7

Table 1
Parameters of recently designed crystal calorimeters

Experiment laboratory	(KTeV) FNAL	BaBar SLAC	BELLE KEK	CMS CERN
Crystal type	CsI	CsI(Tl)	CsI(Tl)	$PbWO_4$
B-field (T)	—	1.5	1.0	4.0
Inner radius (m)	—	1.0	1.25	1.29
Number of crystals	3300	6580	8800	83300
Crystal depth (X_0)	27	16–17.5	16.2	25
Crystal volume (m^3)	2	5.9	9.5	11
Light output (p.e./MeV)	40	5000	5000	2
Photosensor	PMT	Si PD	Si PD	APD[a]
Gain of photosensor	4000	1	1	50
Noise per channel (MeV)	Small	0.15	0.2	30
Dynamic range	10^4	10^4	10^4	10^5

[a]Avalanche photodiode.

notes that each of these calorimeters requires several cubic meters of high-quality crystals.

The unique physics capability of the crystal calorimetry is the result of its superb energy resolution, hermetic coverage and fine granularity [15]. In future high-energy experiments, however, crystal calorimetry faces a new challenge: the radiation damage caused by the increased center of mass energy and luminosity. While the dose rate is expected to be a few rad per day for CsI(Tl) crystals at two B Factories, it would reach 15–500 rad/h for $PbWO_4$ crystals at LHC.

This paper discusses effects of radiation damage in scintillating crystals, several important issues related to the precision of a crystal calorimeter in radiation, and the cause and cure of the radiation damage in crystals. Section 2 gives a brief description of crystal scintillators commonly used in high-energy and nuclear physics experiment. The radiation damage phenomenon is discussed in Section 3 with particular emphasis given to the light response uniformity which is the key issue for achieving and preserving crystal precision in situ. Section 4 discusses the damage mechanism for alkali halides, such as BaF_2 and CsI. Section 5 addresses the oxides, such as bismuth gemanade ($Bi_4Ge_3O_{12}$, BGO) and $PbWO_4$. Finally, a summary is given in Section 6.

All measurements, except specified otherwise in the text, were carried out at Caltech with samples from Beijing Glass Research Institute (BGRI) in Beijing [16], Bogoroditsk Techno-Chemical Plant (BTCP) in Russia [17], Crismatec in France [18], Hilger in Margate, UK [19], Amcrys-H in Khar'kov, Ukraine [20] and Shanghai Institute of Ceramics (SIC) in Shanghai [21].

2. Commonly used crystal scintillators

Table 2 lists the basic properties of some heavy crystal scintillators: NaI(Tl), CsI(Tl), undoped CsI, BaF_2, BGO and $PbWO_4$. All these crystals have been used in high-energy and nuclear physics experiments, and are available in large quantity. The CsI(Tl) crystal is known to have high light yield, and is widely used. Its photon yield per MeV energy deposition exceeds that of NaI(Tl). The relative light yield of 45% listed in the table is due to the quantum efficiency of the Bi–alkali cathode at its emission peak (7%), which is about $\frac{1}{3}$, as compared to 20% of NaI(Tl). The $PbWO_4$ crystal is distinguished with its high density and small radiation length and Moliere radius, and therefore was chosen by the CMS experiment to construct a compact crystal calorimeter. The low light yield of $PbWO_4$ can be overcome by gains of the photodetector, such as the PMT and avalanche photodiode (APD).

3. Radiation damage in scintillating crystals

All known crystal scintillators suffer from radiation damage. The most common damage phenomenon is the appearance of radiation-induced absorption bands caused by color center formation. The absorption bands reduce crystal's light attenuation length (LAL), and hence the light output. The color center formation, however, may or may not cause a degradation of the *light response uniformity*. The radiation also causes phosphorescence (afterglow), which leads to an increase of readout noise. Additional effect may include a reduced intrinsic scintillation light yield (damage of the scintillation mechanism), which would lead to a reduced light

Table 2
Properties of some heavy crystal scintillators

Crystal	NaI(Tl)	CsI(Tl)	CsI	BaF_2	BGO	$PbWO_4$
Density (g/cm^3)	3.67	4.51	4.51	4.89	7.13	8.3
Melting point (°C)	651	621	621	1280	1050	1123
Radiation length (cm)	2.59	1.85	1.85	2.06	1.12	0.9
Moliere radius (cm)	4.8	3.5	3.5	3.4	2.3	2.0
Interaction length (cm)	41.4	37.0	37.0	29.9	21.8	18
Refractive index[a]	1.85	1.79	1.95	1.50	2.15	2.2
Hygroscopicity	Yes	Slight	Slight	No	No	No
Luminescence[b] (nm)	410	560	420	300	480	500
(at Peak)			310	220		500
Decay time[b] (ns)	230	1300	35	630	300	50
			6	0.9		10
Light yield[b,c]	100	45	5.6	21	9	0.3
			2.3	2.7		0.4
$d(LY)/dT$[b,d] (%/°C)	~ 0	0.3	− 0.6	− 2	− 1.6	− 1.9
				~ 0		

[a]At the wavelength of the emission maximum.
[b]Top line: slow component, bottom line: fast component.
[c]Relative and measured with a PMT with a Bi–alkali cathode.
[d]At room temperature.

output and a deformation of the light response uniformity. The damage may recover under room temperature, which leads to the *dose rate dependence* [22]. Finally, thermal annealing and optical bleaching may be effective in eliminating color centers in the crystal.

In previous studies, we conclude that the scintillation mechanism of BGO [23], BaF_2 [24], CsI(Tl) [25] and $PbWO_4$ [26] are not damaged, and the consequence of the radiation-induced phosphorescence is negligible for BaF_2 [24] and $PbWO_4$ [27,28]. It is also known that the damage in BGO [23], BaF_2 [24] and $PbWO_4$ [27,28] are thermally annealable, as well as optically bleach-able, while it is not in CsI [25]. Because of the scope limit of this report, our discussion is concentrated on the main consequence of the radiation damage: the radiation-induced absorption.

3.1. Radiation-induced absorption

The most common damage in scintillating crystals is the radiation-induced color center formation, which reduces the light attenuation length and thus the light output. Depending on the type of the defects in the crystal, the color centers may be electrons located in anion vacancies (F center), or holes located in cation vacancies (V center), or interstitial anion atoms (H center) or ions (I center). Radiation-induced color centers may be observed by measurement of crystal's transmittance. Fig. 1 shows the longitudinal transmittance of three full size (~ 30 cm long) CsI(Tl) samples [25]. The radiation-induced absorption bands are clearly identified in samples BGRI-2 and SIC-4, but is not seen in sample SIC-5, which was grown with a special scavenger in the melt to remove the oxygen contamination. The identified absorption bands centered at 850, 560, 520 and 440 nm are commonly attributed to F, F′, F″ and F‴ centers, respectively.

Fig. 2 shows the longitudinal transmittance of four large size (~ 20 cm long) $PbWO_4$ samples [26]. The radiation-induced absorption bands in $PbWO_4$ are broad, and can be seen in all four samples BTCP-767, 1015, 1018 and SIC-66. A more detailed discussion of color centers can be found in Ref. [29].

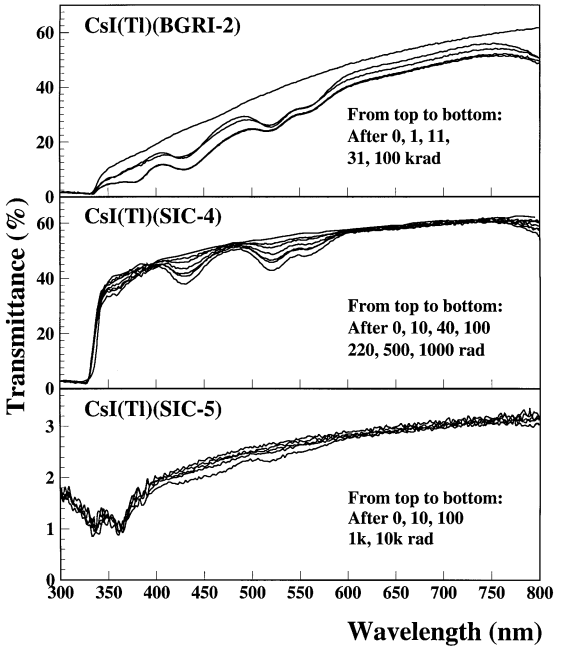

Fig. 1. Longitudinal transmittance of CsI(Tl) samples, showing radiation-induced absorption bands.

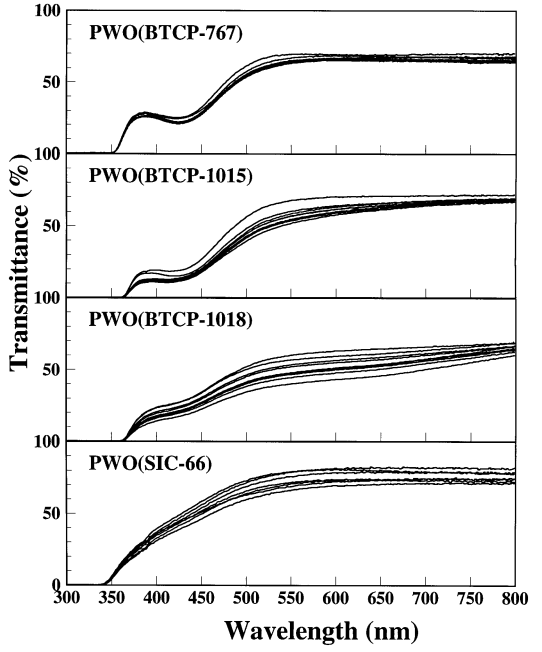

Fig. 2. Longitudinal transmittance of $PbWO_4$ samples, showing radiation-induced absorption bands.

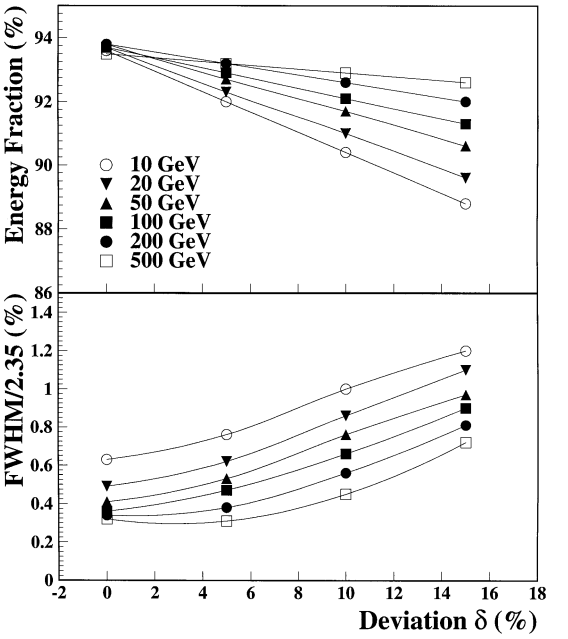

Fig. 3. The effect of light response uniformity predicted by a GEANT simulation.

3.2. Light response uniformity

An adequate light response uniformity profile is the key to the precision of a crystal calorimeter. The effect of the light response uniformity to the energy resolution has been studied by full GEANT simulations for each designed crystal calorimeter. Fig. 3 [24] shows a GEANT prediction for the energy fraction (top figure) and the intrinsic energy resolution (bottom figure) calculated by summing the energies deposited in a 3×3 sub-array, consisting of tapered BaF_2 crystals of 25 radiation length, as a function of the light response uniformity. In this simulation, the light response (y) of the crystal was parametrized as a normalized linear function

$$\frac{y}{y_{\mathrm{mid}}} = 1 + \delta(x/x_{\mathrm{mid}} - 1), \tag{1}$$

where y_{mid} represents the light response at the middle of the crystal, δ represents the deviation of the light response uniformity, and x is the distance

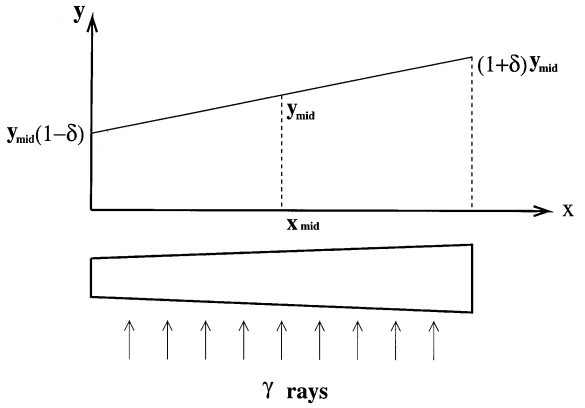

Fig. 4. A schematic showing the light response uniformity definition and its laboratory measurement.

from the small (front) end of a tapered crystal. Fig. 4 shows the definition of the light response uniformity in this simulation and a schematic illustrating its measurement in laboratory by shooting a point γ-ray source at different locations of a tapered crystal.

While the degradation of the amplitude of the light output can be inter-calibrated, the loss of the energy resolution, caused by the degradation of light response uniformity is not recoverable. To preserve crystal's intrinsic energy resolution the light response uniformity thus must be kept within tolerance. According to the above simulation, the δ value is required to be less than 5% so that its contribution to the constant term of the energy resolution is less than 0.5%. Other detailed studies, such as a simulation for BaF_2 crystals using many different functional forms of the light response nonuniformity [30] and a recent simulation for CMS $PbWO_4$ crystals [31], confirmed this conclusion.

Because of the non-uniform dose profile in crystals, caused by energy deposition of particles in experiment, a damage to the scintillation mechanism would cause a distortion of the light response uniformity and thus unrecoverable degradation of the energy resolution. The radiation-induced absorption, however, may or may not cause a severe distortion of the light response uniformity.

Fig. 5 and Fig. 6 show the light response uniformity as a function of accumulated dose for a full

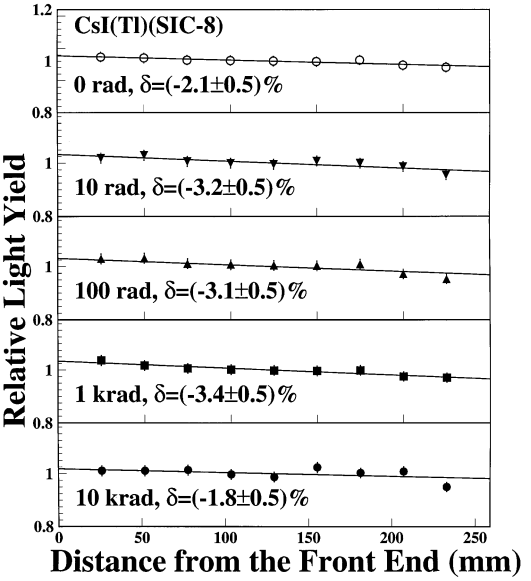

Fig. 5. The light response uniformities are shown as a function of integrated dose for a full size CsI(Tl) sample.

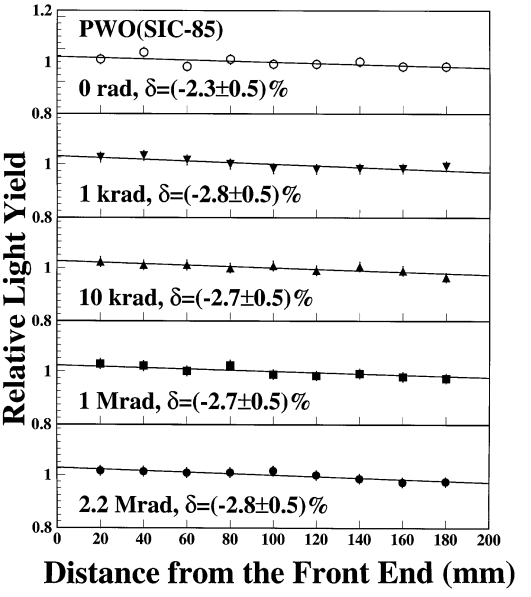

Fig. 6. The light response uniformities are shown as a function of integrated dose for a full size $PbWO_4$ (right) sample.

size CsI(Tl) (~ 30 cm) and a full size $PbWO_4$ (~ 20 cm) crystals, respectively. The pulse heights measured in nine points evenly distributed along the longitudinal axis of the crystal is fit to Eq. (1). This figure shows clearly that the slope (δ) does not change up to 10 krad for the CsI(Tl) sample and to 2.2 Mrad for the $PbWO_4$ sample. The result of CsI(Tl) sample confirms that the CsI(Tl) scintillation mechanism is not damaged, since only the front few cm of the sample was subjected to the radiation dose in this experiment, where a high intensity ^{60}Co source was used to illuminate the front face of the crystal. Although the $PbWO_4$ sample was subjected to a uniform irradiation, an experiment of irradiating only the middle 10 cm of a $PbWO_4$ crystal led to the same result, confirming that the $PbWO_4$ scintillation mechanism is also not damaged. These two samples are example of crystals of good quality. The light response uniformity profile does change under irradiation for crystals of poor quality [25,26].

The result of this laboratory measurement was later confirmed by a beam test for a $PbWO_4$ crystal array at CERN. Intensive electron beam was used to irradiate crystals. Fig. 7 shows that no degradation of energy resolution was found for a sample SIC 69 before and after beam irradiation with an integrated dose of 650 rad [32].

These results are understood by a detailed ray-tracing simulation, as the intensity of all light rays

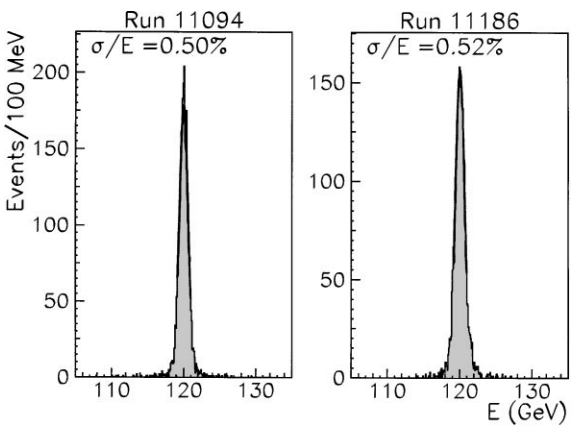

Fig. 7. Response of a sample SIC 69 to 120 GeV electrons as shown before (left) and after (right) 650 rad irradiation.

attenuates similarly after passing through the same radiation-induced absorption zone in the crystal. The exact geometry of a full size $PbWO_4$ crystal ($2^2 \times 23 \times 2.3^2$ cm) was used in this simulation. The refractive index of $PbWO_4$ [33] was assumed to be a tensor, and the polarization of the light ray is taken into account. The simulation was carried out for two photo-detectors: a PMT and an APD. While the PMT covers the full back face of the crystal, only 3.7% of the back area of the crystal was covered by the APD of $\varnothing$ 5 mm diameter. The optical coupling between photo-detectors and the crystal was assumed to have a refractive index of 1.5. The crystal was assumed to be wrapped with Tyvek paper for all surfaces except the part covered by the detector. The interface between Tyvek paper and crystal surface was assumed to have a thin air gap and a reflectivity of 0.9, and a defused reflection with the reflection angle smeared with a Gaussian width of 0.5 radian. Photons were generated isotropically in the crystal and were traced all the way. The accumulated path length of the photon was used together with the assumed light attenuation length to calculate the weight of the photon. Photons were followed until either absorbed by the photo-detector or escaped from the crystal, or its weight is less than e^{-5}. Finally, the light collection efficiency (y) was obtained by averaging all weights of photons absorbed by the photo-detector, and was fitted to the Eq. (1).

Table 3 lists the numerical result together with statistical errors of the simulation. As can be seen from this table, the slope of the light response uniformity (δ) is entirely determined by the crystal geometry, if the light attenuation length is long enough. The table also shows that the light output (y_{mid}) of a detector covering a smaller fraction of the back face (APD) is more sensitive to the degradation of the light attenuation length, or radiation-induced color centers.

Since the degradation of the amplitude of the light output can be inter-calibrated with physics events or by a light monitoring system, if it is caused by optical absorption, to preserve crystal precision in situ two necessary conditions must be satisfied. First, crystal's scintillation mechanism must not be damaged and second, crystal's initial light attenuation length must be long enough and

Table 3
Result of a ray-tracing simulation for a full-size $PbWO_4$ crystal

LAL (cm)	20	40	60	80	200	400
Full face photo-detector, covering 100% back face						
y_{mid} (%)	9.5 ± 0.2	15.7 ± 0.4	19.2 ± 0.5	21.6 ± 0.6	26.9 ± 0.7	29.1 ± 0.8
δ (%)	23 ± 1	-5 ± 1	-11 ± 1	-15 ± 1	-15 ± 1	-16 ± 1
$\varnothing$ 5 mm photo-detector, covering 3.7% back face						
y_{mid} (%)	0.38 ± 0.04	0.74 ± 0.084	1.1 ± 0.1	1.4 ± 0.2	3.0 ± 0.3	5.1 ± 0.3
δ (%)	23 ± 4	-4 ± 4	-12 ± 4	-16 ± 4	-17 ± 3	-16 ± 2
$\frac{y_{mid}(\varnothing 5mm)}{y_{mid}(Full)}$ (%)	4.0	4.7	5.7	6.5	11	17.5

the density of radiation-induced color center must be low enough, so that the light response uniformity does not degrade in situ.

3.3. Damage recovery

The radiation damage in crystal may recover at room temperature – a consequence of room temperature thermal annealing. The recovery speed, however, depends on the depth of the traps. A slow recovery would ease the calibration requirement, therefore it is preferred for crystals to be used in a radiation environment. It is known that damage in BaF_2 [24] and CsI [25] recovers at an extremely slow speed, while BGO [23] and $PbWO_4$ [27,28] do recover at a speed of orders of few hours to few weeks.

Fig. 8 shows the recovery speed of less than 0.5% per day for three full size ($\sim$ 30 cm) CsI(Tl) samples after a 100 krad irradiation, which indicates that the radiation-induced color centers in CsI(Tl) are caused by deep traps. The thermal annealing did not accelerate the recovery when below 300°C, and made sample BGRI-2 milky and produced no more scintillation light beyond 300°C. This was explained by the drift of the thallium luminescence centers out of the CsI(Tl) lattice at 300°C. Because of this slow recovery, the required accuracy of inter-calibration may be provided by physics in situ, e.g. Bhabha events, in a few hours.

Fig. 9 shows the damage recovery for a full size (23 cm) $PbWO_4$ sample BTCP-1015 after a dose of

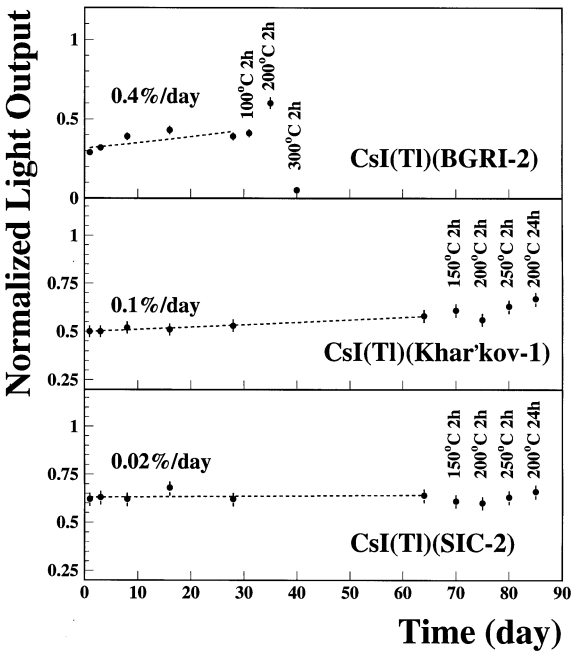

Fig. 8. The recovery of radiation damage is shown for three full size ($\sim$ 30 cm) CsI(Tl) crystals after 100 krad irradiation.

1 Mrad. The top plot shows the recovery in the transmittance as a function of wavelength. The bottom plot shows normalized light output as a function of time after irradiation. The solid line in the light output plot is a fit to an exponential with a time constant of 160 h. Because of this damage

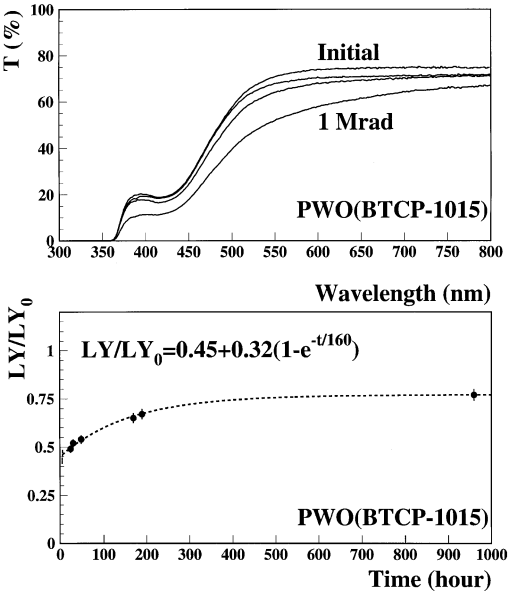

Fig. 9. The recovery of radiation damage is shown for a full size (23 cm) $PbWO_4$ crystal after 1 Mrad irradiation.

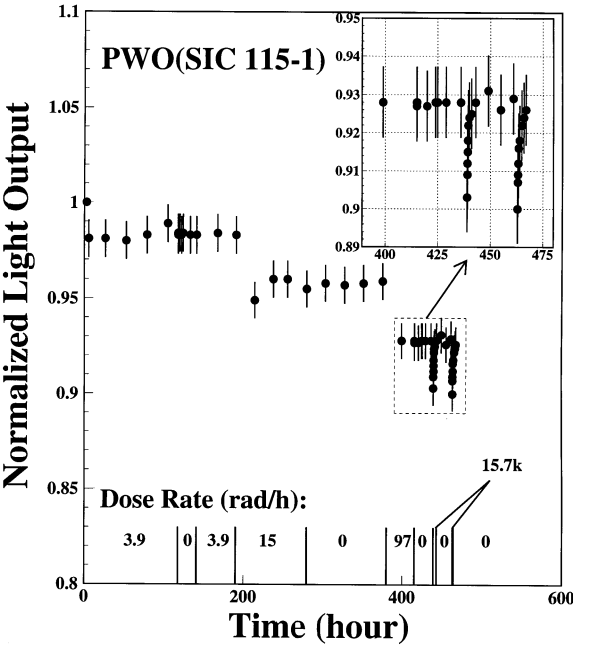

Fig. 10. The dose rate dependence is shown for a 5 cm $PbWO_4$ sample SIC 115-1.

and recovery, special attention should be paid to the stability of a $PbWO_4$ calorimeter in situ.

3.4. Dose rate dependence

If both annihilation and creation coexist, the color center density at the equilibrium depends on the dose rate applied. Assuming the annihilation speed of color center i is proportional to a constant a_i and its creation speed is proportional to a constant b_i and the dose rate (R), the differential change of color center density when both processes coexist can be written as [34,35]

$$\mathrm{d}D = \sum_{i=1}^{n} \{ -a_i D_i + (D_i^{\mathrm{all}} - D_i) b_i R \} \, \mathrm{d}t, \tag{2}$$

where D_i is the density of the color center i in the crystal and the summation goes through all centers. The solution of Eq. (2) is

$$D = \sum_{i=1}^{n} \left\{ \frac{b_i R D_i^{\mathrm{all}}}{a_i + b_i R} [1 - \mathrm{e}^{-(a_i + b_i R)t}] + D_i^0 \mathrm{e}^{-(a_i + b_i R)t} \right\}, \tag{3}$$

where D_i^{all} is the total density of the trap related to the center i and D_i^0 is its initial density. The color center density in equilibrium (D_{eq}) thus depends on the dose rate (R).

$$D_{\mathrm{eq}} = \sum_{i=1}^{n} \frac{b_i R D_i^{\mathrm{all}}}{a_i + b_i R}, \tag{4}$$

Fig. 10 shows the entire history of a light output measurement for a 5 cm $PbWO_4$ sample SIC 115-1 in 20 days. The measured light output was normalized to that before irradiation, and was plotted as a function of the time of the measurement. The dose rate and integrated dose are also shown in the figure. There were periods when dose rate was shown as zero, indicating a recovery test. As shown in the figure, the level of $PbWO_4$ damage is indeed dose rate dependent, and the fast recovery (in order of a few hours) was observed only when dose rate is 15.7 krad/h, as shown in the inset.

If the recovery speed (a) is slow, however, the dose rate dependence would be less important, the color center density in the equilibrium would

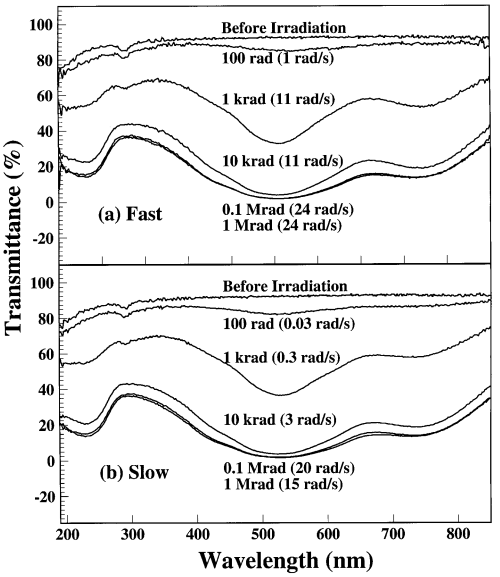

Fig. 11. No dose rate dependence was observed for a 25 cm BaF_2 sample.

depend less on the dose rate. The extrema is not dose rate dependent, as shown in Eq. (5)

$$D'_{\mathrm{eq}} = \sum_{i=1}^{n} D_i^{\mathrm{all}}. \tag{5}$$

Fig. 11 [21] shows the transmittance as a function of wavelength for a full size (25 cm) BaF_2 sample before and after 100, 1, 10, 100 k and 1 M rad irradiations (from top to bottom) under a fast (a) and a slow (b) dose rate. While the fast rate is up to a factor of three higher than the slow rate, the damage levels for the same integrated dose are identical. This was expected, since no recovery at room temperature was observed for BaF_2. Because of this dose rate dependence, an adequate rad-hard specification for $PbWO_4$ crystals would refer to a level of light output degradation under a specific dose rate expected at LHC of full luminosity.

4. Damage mechanism in alkali halides

Material analysis is very important in identifying the radiation damage mechanism. We tried the Glow Discharge Mass Spectroscopy (GDMS) analysis in Charles Evans and Associates [36], looking for correlations between the trace impurities in the CsI(Tl) crystals and their radiation hardness. Samples were taken 3–5 mm below the surface of the crystal to avoid surface contamination. A survey of 76 elements, including all the lanthanides, indicates that there are no obvious correlations between the detected trace impurities and crystal's susceptibility to the radiation damage. This indicates an important role of oxygen contamination which cannot be determined by GDMS.

The oxygen contamination is known to cause radiation damage in alkali halide scintillators. In BaF_2 [24], for example, hydroxyl (OH^-) may be introduced into crystal through a hydrolysis process, and latter decomposed to interstitial and substitutional centers by radiation through a radiolysis process. Eq. (6) shows a scenario of this process:

$$OH^- \rightarrow H_i^0 + O_s^- \quad \text{or} \quad H_s^- + O_i^0, \tag{6}$$

where subscript i and s refer to interstitial and substitutional centers, respectively. Both the O_s^- center and the U center (H_s^-) were identified [24].

Following the BaF_2 experience, effort was made to remove oxygen contamination in CsI(Tl) crystals. An approach was taken at SIC: using a scavenger, such as Pb for BaF_2, to remove oxygen contamination. A significant improvement of the radiation hardness was achieved for CsI(Tl) crystals produced taking this approach [25].

Fig. 12 shows the light output as a function of accumulated dose for full size CsI(Tl) samples, and compared to the BaBar radiation hardness specification (solid line). While the late samples SIC-5, 6, 7 and 8 (with scavenger) satisfy the BaBar specification, early samples SIC-2 and 4 did not. It is understood that the function of the scavenger is to form oxide with density less than CsI, so that the oxide will migrate to the top of the ingot during the growing process, similar to the zone-refining process. By doing so, both oxygen and scavenger are removed from the crystal.

Additional analysis was carried out to quantitatively identify the oxygen contamination in CsI(Tl) samples. We first tried the Gas Fusion (LECO) at Shiva Technologies West, Inc. [37], and found that

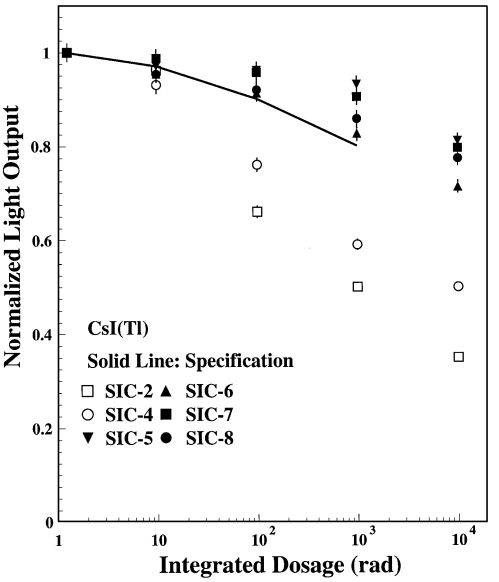

Fig. 12. The progress of CsI(Tl) radiation hardness is shown for full size (~ 30 cm) CsI(Tl) samples from SIC together with the rad-hard specification of BaBar experiment.

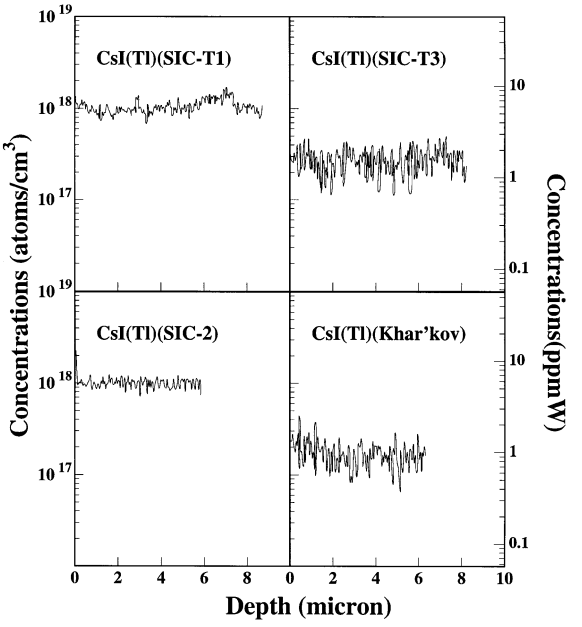

Fig. 13. The depth profile of oxygen contamination is shown for two rad-soft CsI(Tl) samples (SIC-T1 and SIC-2) and two rad-hard samples (SIC-T3 and Khar'kov).

the oxygen contamination in all CsI(Tl) samples is below the LECO detection limit: 50 ppm. We then tried Secondary Ionization Mass Spectroscopy (SIMS) at Charles Evans and Associates. A Cs ion beam of 6 keV and 50 nA was used to bombard the CsI(Tl) sample. All samples were freshly cleaved prior being loaded to the UHV chamber. An area of $0.15 \times 0.15\,mm^2$ on the cleaved surface was analyzed. To further avoid surface contamination, the starting point of the analysis was at about 10 μm deep inside the fresh cleaved surface. Fig. 13 shows depth profile of oxygen contamination for two rad-soft (SIC-T1 and SIC-2) and two rad-hard (SIC-T3 and Khar'kov) CsI(Tl) samples. Crystals with poor radiation resistance have oxygen contamination of 10^{18} atoms/cm^3 or 5.7 ppmW, which is 5 times higher than the background count (2×10^{17} atoms/cm^3, or 1.4 ppmw). The radiation damage in CsI(Tl) is indeed caused by oxygen contamination.

5. Damage mechanism in oxides

Similarly, the GDMS analysis at Charles Evans and Associates found no specific correlations between the detected trace impurities in $PbWO_4$ crystals and crystal's susceptibility to the radiation damage [27]. This indicates an important role of defects in the crystal, such as oxygen vacancies which cannot be determined by GDMS. Table 4 lists the result of GDMS analysis for trace elements (ppmw) in several $PbWO_4$ samples.

The result of GDMS analysis, however, revealed that the presence of slow scintillation component in $PbWO_4$ is due to the Mo contamination, as shown in Fig. 14. A similar observation was earlier reported by Kobayashi [38]. This correlation is easy to be understood, since lead molybdate ($PbMoO_4$) is a known scintillator with slow (~ 10 μs) decay time. After removing Mo and other cation contamination from the raw material, $PbWO_4$ crystals produced at both BTCP and SIC have a significantly reduced slow component.

Crystal defects, such as oxygen vacancies, is known to cause radiation damage in oxide scintillators. In BGO, for example, three common radiation-induced absorption bands at 2.3, 3.0 and

Table 4
Result of GDMS trace analysis (ppmw) for $PbWO_4$ samples

Element	Na	Si	K	Ca	Nb	Mo	Ba	TM[a]	RE[b]
BTCP-478	1.8	3.0	2.5	1.3	2.4	4.6	0.24	1.2	0.13
BTCP-728	3.2	< 0.7	< 0.3	5.5	3.9	8.9	0.82	< 1.0	0.28
BTCP-767	9.3	42	0.52	0.97	7.8	16	0.40	< 0.4	0.11
BTCP-768	1.8	51	0.52	2.4	6.9	15	0.51	< 0.4	0.12
BTCP-1015	2.8	1.5	1.9	5.5	7.9	120	0.16	1.8	0.11
BTCP-1022	3.1	1.8	1.7	7.7	10	100	0.16	1.6	0.10
SIC-34	3.0	1.3	3.3	2.7	< 0.002	14	1.0	1.3	0.18
SIC-41	1.7	0.8	3.4	10	< 0.001	18	3.8	1.4	0.15
SIC-O1	0.5	0.4	0.5	0.4	< 0.05	1.1	0.02	0.02	< 0.05
SIC-O2	0.1	0.02	0.2	0.2	< 0.05	0.6	0.03	0.06	< 0.05

[a]Sum of transition metals.
[b]Sum of rare earths.

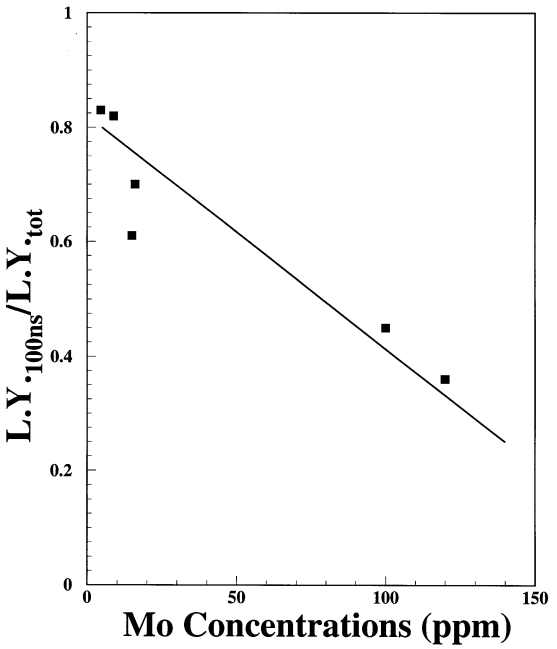

Fig. 14. The correlation between Mo contamination and the fraction of fast scintillation component.

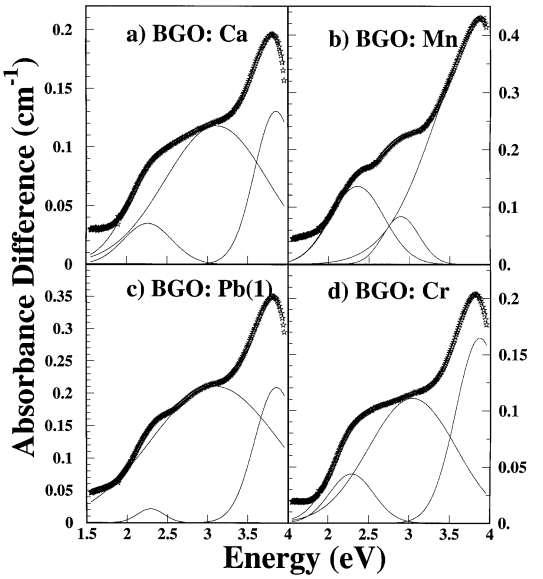

Fig. 15. Radiation-induced absorption spectra of four doped BGO samples ($1 \times 3 \times 1$ cm) are decomposed into three common absorption bands.

3.8 eV were found in a series of 24 doped samples [23], indicating defect-related color centers, such as oxygen vacancies. Fig. 15 shows the radiation-induced absorption spectra for four small ($1 \times 3 \times 1$ cm) BGO samples doped with Ca, Mn, Pb and Cr, respectively. Although the shape of these radiation-induced absorption bands are rather different, a decomposition showed three common absorption bands at the same energy and with the same width.

Following the BGO experience, effort was made to reduce oxygen vacancies in $PbWO_4$ crystals. An

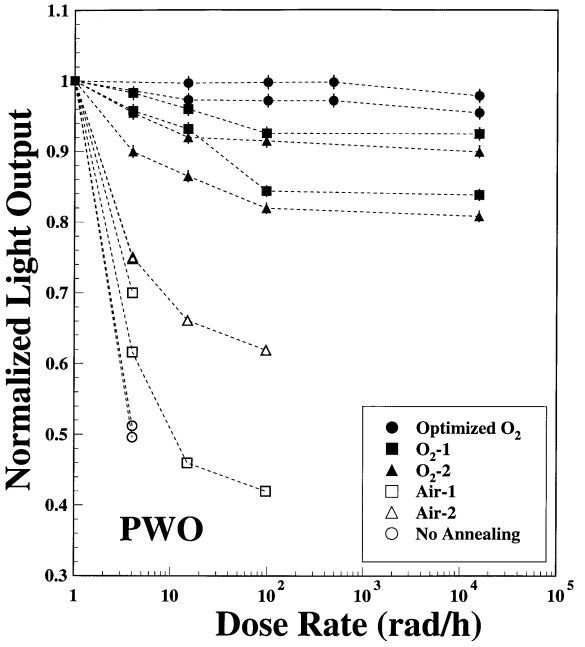

Fig. 16. Normalized light output at the equilibrium is shown as a function of the dose rate for six pairs of small ($2 \times 5 \times 2$ cm) $PbWO_4$ samples treated with different post-growing thermal annealing conditions.

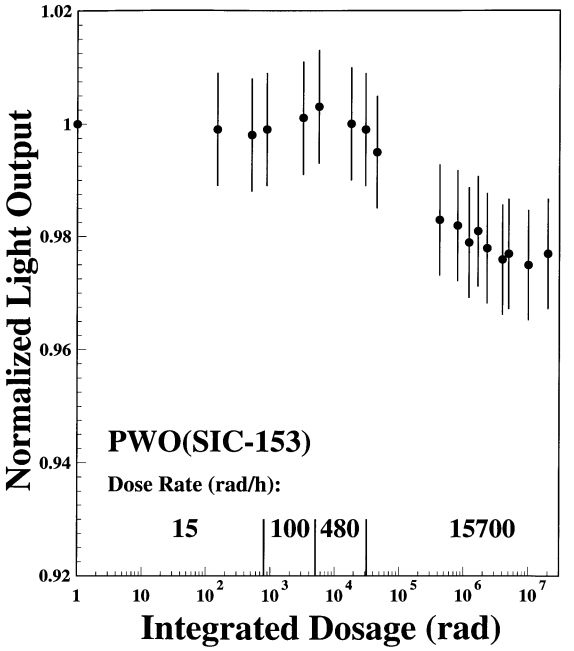

Fig. 17. The normalized light output of a small ($2 \times 5 \times 2$ cm) $PbWO_4$ sample SIC 153 is shown as a function of the integrated dose.

approach was taken at SIC: oxygen compensation through post-growth thermal annealing in an oxygen-rich atmosphere. Significant improvement of radiation hardness was achieved. Fig. 16 shows the normalized light output at the equilibrium as a function of the dose rate for 6 pairs of small ($2 \times 5 \times 2$) $PbWO_4$ samples, which were treated with different oxygen compensation conditions. The result shows that samples annealed under different conditions have much different behavior. Samples, which were not annealed, have the worst radiation hardness. Samples annealed in oxygen are more radiation hard than that in air. Samples, which were annealed under the optimized oxygen conditions, are the best.

Samples treated under the optimized oxygen annealing are radiation hard. Fig. 17 shows the normalized light output as a function of integrated dose up to 20 Mrad for a small ($2 \times 5 \times 2$) sample 153. This sample showed no degradation in light output under a dose rate of below 480 rad/h, and had only 2% degradation under an extremely high dose rate of 15.7 krad/h. Samples of this quality certainly can satisfy the most stringent radiation hardness specification for CMS.

Further analysis was carried out to quantitatively identify the stoichiometry deviation and oxygen vacancies in $PbWO_4$ samples. We first tried Particle-Induced X-ray Emission (PIXE) and quantitative wavelength-dispersive Electron Micro-Probe Analysis (EMPA) for $PbWO_4$ crystals in Charles Evans and Associates. Indeed, crystals with poor radiation hardness were found to have a non-stoichiometric W/Pb ratio [27,28]. However, both PIXE and EMPA did not provide oxygen analysis.

The direct observation of oxygen vacancies requires a measurement of the complete stoichiometric ratio of Pb : W : O in $PbWO_4$ samples. X-ray Photoelectron Spectroscopy (XPS) was tried at Charles Evens and Associates [39]. It, however, was found to be very difficult due to the systematic uncertainty in oxygen analysis. Effort has also been made to directly identify oxygen vacancies by Electron Paramagnetic Resonance (ESR) and

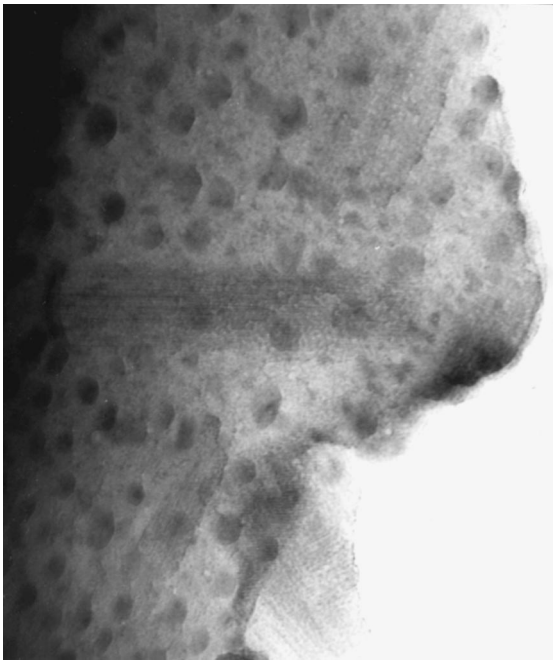

Fig. 18. TEM pictures of a $PbWO_4$ crystal of poor radiation hardness, showing clearly the black spots of a diameter of 5–10 nm related to oxygen vacancies.

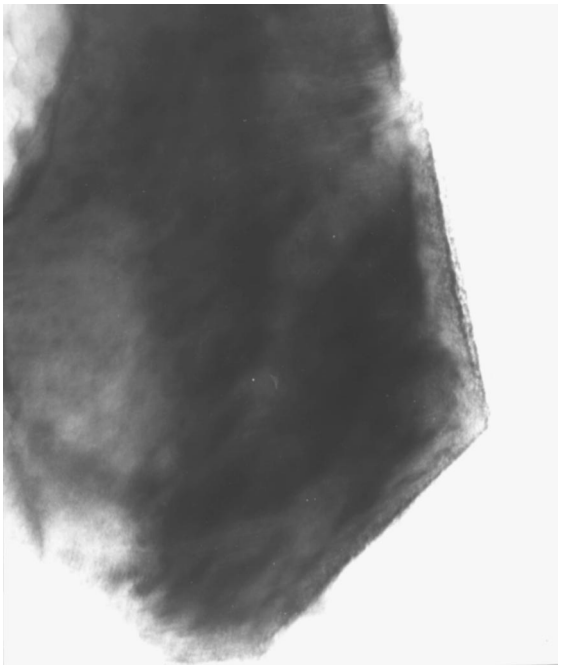

Fig. 19. TEM pictures of a $PbWO_4$ crystal of good radiation hardness, showing no metallic concentration.

Electron–Nuclear Double Resonance (ENDOR) through observing unpaired electrons. It, however, was also difficult to reach a quantitative conclusion.

By using Transmission Electron Microscopy (TEM) coupled to Energy Dispersion Spectrometry (EDS), a localized stoichiometry analysis was possible to identify oxygen vacancies. A TOPCON-002B Scope was first used at 200 kV and 10 μA. Samples were powdered of an average grain size of a few μm, and then placed on a sustaining membrane. With a spatial resolution of 2 Å, the lattice structure of $PbWO_4$ crystals was clearly visible. Fig. 18 shows a TEM picture taken for a sample with poor radiation hardness. Black spots of a diameter of 5–10 nm were clearly seen in the picture. On the other hand, samples with good radiation hardness show stable TEM picture with no black spots, as shown in Fig. 19.

By employing a TEM with EDS system, a localized stoichiometry analysis was carried out at SIC [40]. The system is a JEOL JEM-2010 scope and a Link ISIS EDS. The spatial resolution of this system allows a localized stoichiometry analysis in a region of a diameter of 0.5 nm [40]. An as grown sample was first analyzed, and black spots were observed. Points inside and surrounding the black spots were analyzed as well as points far away from the black spots. The uncertainty of the analysis is typically 15%. The resultant atomic fractions (%) at these areas are listed in Table 5. A clear deviation from the atomic stoichiometry of $O:W:Pb = 66:17:17$ was observed in the center of these black spots, pointing to a severe deficit of oxygen component. In the peripheral area, the oxygen deficit was less, but still significant. There was no oxygen deficit observed in the area far away from the black spots. As a comparison, the same sample after oxygen compensation was re-analyzed. No black spot was found. The result of the analysis is also listed in Table 5. In all randomly selected points no stoichiometry deviation was observed. This analysis thus clearly identified oxygen vacancies in $PbWO_4$ samples of poor radiation hardness.

Table 5
Atomic fraction (%) of O, W and Pb in $PbWO_4$ samples measured by TEM/EDS [34]

As grown sample				
Element	Black spot	Peripheral	$Matrix_1$	$Matrix_2$
O	1.5	15.8	60.8	63.2
W	50.8	44.3	19.6	18.4
Pb	47.7	39.9	19.6	18.4
The same sample after oxygen compensation				
Element	$Point_1$	$Point_2$	$Point_3$	$Point_4$
O	59.0	66.4	57.4	66.7
W	21.0	16.5	21.3	16.8
Pb	20.0	17.1	21.3	16.5

Table 6
Radiation damage effect in crystal scintillators

Crystal	CsI(Tl)	CsI	BaF_2	BGO	$PbWO_4$
Color centers	Yes	Yes	Yes	Yes	Yes
Phosphorescence	Yes	Yes	Yes	Yes	Yes
Scintillation	No	No	No	No	No
Recovery at room temperature	Slow	Slow	No	Yes	Yes
Dose rate dependence	No	No	No	Yes	Yes
Thermal annealing	No	No	Yes	Yes	Yes
Optical bleaching	No	No	Yes	Yes	Yes

6. Summary

Crystal calorimeters in future high-energy colliders will operate in a severe radiation environment caused by the increased center of mass energy and luminosity. Despite much experience and expertise accumulated in the last decade, crystal calorimetry is facing a new challenge. Without stringent quality control, crystals would suffer from significant radiation damage, leading to a degraded performance.

Possible effects of radiation damage in scintillating crystals include (1) radiation-induced absorption; (2) radiation-induced phosphorescence, and may be (3) damage in scintillation mechanism. The predominant radiation damage effect in crystal scintillators is the radiation-induced absorption, or color center formation, not the loss of scintillation light yield. Table 6 summarizes radiation damage effect in commonly used crystal scintillators.

It is understood that crystal scintillators for precision calorimetry must preserve their light response uniformity under irradiation, which requires a long enough initial light attenuation length and a low enough color center density. With such crystals, a precision light monitoring may function as inter-calibrations.

The radiation damage in alkali halides is understood to be caused by the oxygen and/or hydroxyl contamination, as evidenced by the SIMS analysis and the effectiveness of the usage of a scavenger in removing oxygen contamination in CsI(Tl) crystals. It is also understood that the stringent specifications for CsI(Tl) crystals to be used to construct calorimeters for two B Factories can be met by mass-produced crystals.

The radiation damage in oxides is understood to be caused by stoichiometry-related defects, e.g. oxygen vacancies, as evidenced by localized stoichiometry analysis by TEM/EDS, and the effectiveness of the oxygen compensation for $PbWO_4$ crystals. It is expected that rad-hard $PbWO_4$ crystals will be developed through the systematic research and development program carried out by CMS physicists in collaboration with crystal manufactures.

Acknowledgements

Measurements at Caltech were carried out by Mr. Q. Deng, H Wu, D.A. Ma, Z.Y. Wei and T.Q. Zhou. Part of the $PbWO_4$-related work was carried out by Dr. C. Woody and his group at Brookhaven National Laboratory. Prof. Z.W. Yin, Drs. G. Cheng and P. Lecoq provided samples described in this report. Many inspiring and interesting discussions with Drs. M. Kobayashi, P.J. Li, J.Y. Liao, D.Z. Shen, C. Woody, and Z.W. Yin are also acknowledged. The author would also like to thank Dr. J.L. Faure for reading and commenting the manuscript. This work is supported in part by U.S.

Department of Energy Grant No. DE-FG03-92-ER40701.

References

[1] M. Oreglia et al., Phys. Rev. D 25 (1982) 2295.
[2] E. Bloom, C. Peck, Ann. Rev. Nucl. Part. Sci. 33 (1983) 143.
[3] T. Böringer et al., Phys. Rev. Lett. 44 (1980) 1111.
[4] G. Mageras et al., Phys. Rev. Lett. 46 (1981) 1115.
[5] L3 Collaboration, Nucl. Instr. and Meth. A 289 (1990) 35.
[6] Y. Kubota et al., Nucl. Instr. and Meth. A 320 (1992) 66.
[7] E. Aker et al., Nucl. Instr. and Meth. A 321 (1992) 69.
[8] K. Arisaka et al., KTeV Design Report, FN-580, January, 1992.
[9] BaBar Collaboration, Technical Design Report, SLAC-R-95-457, 1995.
[10] BELLE Collaboration, Technical Design Report, KEK Report 95-1, 1995.
[11] CMS Collaboration, The Electromagnetic Calorimeter Technical Design Report, CERN/LHCC 97-33, 1997.
[12] S. Mrenna et al., CALT 68-1856, June 1993.
[13] R.Y. Zhu, H. Yamammoto, CALT 68-1802, July 1992.
[14] R.Y. Zhu, CALT 68-1777, November 1991.
[15] G. Gratta et al., Ann. Rev. Nucl. Part. Sci. 44 (1994) 453.
[16] Beijing Glass Research Institute is a research institution in Beijing, 1 Dongdadi Chongwenmen Wai, Beijing 100062, China.
[17] Bogoroditsk Techno-Chemical Plant, Russia.
[18] The Crismatec is a subsidiary of Saint-Gobain Ceramics Industries, 77794 Nemous Cedex, France.
[19] The Hilger Analytical Limited is in Westwood, Margate, Kent CT9 4JL United Kingdom.
[20] The Amcrys-H is the commercial branch of the Institute for Single Crystals Research, 60 Lenin Ave, Khar'kov, Ukraine.
[21] Shanghai Institute of Ceramics is a research institution belong to the Chinse Academy of Sciences, 1295 Ding Xi Road, Shanghai 200050, China.
[22] R.Y. Zhu, IEEE Trans. Nucl. Sci. NS-44 (1997) 468.
[23] R.Y. Zhu et al., Nucl. Instr. and Meth. A 302 (1991) 69.
[24] R.Y. Zhu, Nucl. Instr. and Meth. A 340 (1994) 442.
[25] R.Y. Zhu et al., in: A. Antonelli et al. (Ed.), Proc. 6th Int. Conf. on Calorimetry in High Energy Physics, Frascati Physics Series 589, 1996.
[26] R.Y. Zhu et al., in: A. Antonelli et al. (Ed.), Proc. 6th Int. Conf. on Calorimetry in High Energy Physics, Frascati Physics Series 577, 1996.
[27] C. Woody et al., in: Proc. SCINT95 Int. Conf. Delft, August 1995 and IEEE-NUCL-S V43 (1996) 1585.
[28] R.Y. Zhu et al., Nucl. Instr. and Meth. A 376 (1996) 319.
[29] There are many literatures discussing color centers in solids, for example, J.H. Crawford, L.M. Slifkin, Point Defects in Solids, Plenum Press, New York, 1972.
[30] K. Shmakov, GEM TN-92-143, August, 1992.
[31] D. Graham, C. Seez, CMS Note 1996-002.
[32] E. Auffray et al., CMS Note 97-099, Nucl. Instr. and Meth., submitted.
[33] G. Bakhshiva, A. Morozov, Sov. J. Opt. Technol. 44 (9) 1977.
[34] D.A. Ma et al., Nucl. Instr. and Meth. A 332 (1993) 113.
[35] D.A. Ma et al., Nucl. Instr. and Meth. A 356 (1995) 309.
[36] Charles Evans & Associates, 301 Chesapeake Drive, Redwood City, CA 94063.
[37] Shiva Technologies West, Inc., 16305 Caputo Drive Suite C, Morgan Hill, CA 95037.
[38] M. Kobayashi et al., Nucl. Instr. and Meth. A 373 (1996) 333.
[39] C. Lazik, private communications.
[40] Z.W. Yin et al., paper in Proc. SCINT97 Int. Conf., Shanghai, September 1997.